J. Fluid Mech. (1981), *vol.* 112, *pp.* 347–362
Printed in Great Britain

The circular hydraulic jump

By A. D. D. CRAIK, R. C. LATHAM,†
Department of Applied Mathematics,
University of St Andrews, Fife KY16 9SS, Scotland
M. J. FAWKES‡ AND P. W. F. GRIBBON
Department of Physics,
University of St Andrews, Fife KY16 9SS, Scotland

(Received 30 October 1980)

The circular hydraulic jump commonly forms on a horizontal plate struck by a vertical jet of liquid. New observations of this phenomenon are described.

A previously unreported instability of the jump is examined. This is shown to arise when the local Reynolds number R_j just ahead of the jump exceeds a critical value of 147. Prior to this instability, the flow behind the jump contains a closed eddy, the length of which decreases to zero as R_j increases towards its critical value. Physical explanations for this flow structure and instability are proposed.

Accurate measurements of liquid depths were made using a light-absorption technique, in which a laser was shone through water containing a strong dye. Liquid depths ahead of and behind the jump were so determined and depth profiles of the jump in the stable regime were obtained.

As the outer depth was increased, the jump closed in on the jet and eventually disappeared: this extinction of the jump is also investigated.

1. Introduction

When a vertical jet of liquid hits a horizontal plane, it spreads out radially in a thin fast-moving film before experiencing a rather rapid increase of depth and reduction of mean speed at a certain radial distance. The change of depth and speed is analogous to that of the bore or hydraulic jump and it has therefore been named the 'circular hydraulic jump' (though, in fact, the transition may be less rapid than this name suggests). Various studies of this familiar phenomenon exist, notably by Watson (1964), Olsson & Turkdogan (1966), Ishigai *et al.* (1977), Bouhadef (1978) and Nakoryakov, Pokusaev & Troyan (1978). The heat-transfer characteristics of such flows, which are of interest for chemical engineering applications, have been studied by Chaudhury (1964) and Ishigai *et al.* (1977).

Watson's (1964) theoretical analysis of the flow ahead of the jump estimates how the velocity profile and film thickness vary with radial distance r. For sufficiently small r (but away from the base of the jet) he predicts a uniform flow velocity modified by a growing Blasius boundary layer on the wall; while, at larger r, when the boundary layer extends to the surface, the velocity profile is given by a similarity solution. To

† Present address: c/o Scottish Widows Trust, Edinburgh.
‡ Present address: c/o British Nuclear Fuels, Chapelcross.

conserve volume flux, the liquid depth first decreases as r increases, because of radial divergence; but it then increases again because of viscous retardation. The radial location $r = r_1$ of the jump depends both on the volume flux and on the downstream depth, and the jump may terminate the flow profile described above at any radius. The approximate location of the jump may be deduced from consideration of continuity of flux and momentum balance. Inviscid theory, which assumes uniform constant velocities before and after the jump, leads to the prediction

$$\frac{r_1 d^2 g a^2}{Q^2} = \frac{1}{\pi^2} - \frac{g d a^4}{2Q^2} \tag{1.1}$$

(see Watson 1964, § 2), where

$$Q = \pi a^2 U_0 = 2\pi r h U_0$$

is the volume flux, a is the jet radius just before impact, U_0 is the *constant* liquid velocity for $r < r_1$ and $h(r)$ is the variable film thickness before the jump. The liquid depth just behind the jump is d and gravitational acceleration is g.

Incorporation of viscous effects (see Watson 1964, § 5) leads to the modified results

$$\frac{r_1 d^2 g a^2}{Q^2} + \frac{a^2}{2\pi^2 r_1 d} = 0{\cdot}01676 \left\{ \left(\frac{r_1}{a}\right)^3 R^{-1} + 0{\cdot}1826 \right\}^{-1} \tag{1.2a}$$

provided $r_1/a \geqslant 0{\cdot}3155 R^{\frac{1}{3}}$ and

$$\frac{r_1 d^2 g a^2}{Q^2} + \frac{a^2}{2\pi^2 r_1 d} = \frac{1}{\pi^2} - 0{\cdot}1297 \left(\frac{r_1}{a}\right)^{\frac{3}{2}} R^{-\frac{1}{2}} \tag{1.2b}$$

when $r_1/a < 0{\cdot}3155 R^{\frac{1}{3}}$. Here, $R = Q/\nu a$ is a Reynolds number defined relative to the radius of the impinging jet. The results (1.2a) and (1.2b) derive from the similarity profile and the Blasius profile respectively and are subject to the additional assumption that $h^2/d^2 \ll 1$, which is normally well satisfied. Since $a^2/2r_1 d = h(r_1)/d$, the second term on the left-hand side of (1.2b) is small compared with π^{-2}. Accordingly, results (1.1) and (1.2b) agree, to order $O(h^2/d^2)$, in the limit $R \to \infty$.

Unfortunately, unlike (1.1), results (1.2a, b) do not yield explicit formulae for the jump radius r_1; but these equations may be readily solved numerically in particular cases. Both (1.2a) and (1.2b) predict that the left-hand side depends on $(r_1/a) R^{-\frac{1}{3}}$ only. Watson's own experimental results and those of others show considerable scatter, but agree broadly with (1.2a, b) provided the liquid flow remains laminar, the greatest discrepancies occurring when d/r_1 exceeds 0·1. For turbulent flow, Watson derived results analogous to (1.2a, b), but agreement with his experiment is then rather less satisfactory. The inviscid result (1.1) is, at best, a very rough approximation. Olsson & Turkdogan (1966) and Ishigai *et al.* (1977) measured liquid-film thicknesses ahead of the jump. Their results are in rough agreement with Watson's theory, but Olsson & Turkdogan (1966) suggest that the similarity solution may not become established until rather larger radii than Watson's theory predicts and also that the surface velocity may remain virtually constant right up to the jump, but with magnitude *less* than that of the impinging jet.

Watson does not consider the detailed flow structure within and behind the jump. But to view the phenomenon as a simple discontinuity in depth and velocity is a great oversimplification: the actual flow structure is complex and varies markedly with changing conditions. Comments on the shape of the liquid surface at the jump are

made by Ishigai *et al.*, who claim to distinguish four categories controlled by the Froude number $Fr \equiv V(gh)^{-\frac{1}{2}}$, where V and h are the mean velocity and the film thickness just ahead of the jump. These are (i) a stable smooth surface supporting a pair of standing waves ($Fr < 2$), (ii) a smooth gradual increase in depth ($2 < Fr < 7$), (iii) a narrower more rounded jump ($7 < Fr < 15$) and (iv) an unstable jump at which air bubbles are constantly entrained ($Fr > 15$). There is a shortage of quantitative data in support of such precise categorization, but there is no doubt that the jump does undergo substantial qualitative changes as the flow parameters vary.

By an ingenious method, Nakoryakov *et al.* (1978) measured the wall shear stress as a function of radius, finding that this becomes negative within the jump region. This indicates a zone of reversed flow near the wall consistent with boundary-layer separation. They also made liquid depth measurements across the jump but found that, over part of the region, 'accuracy... was inadequate owing to waves at the liquid surface'.

Bouhadef's (1978) theoretical treatment of the flow ahead of the jump appears less satisfactory than Watson's, the velocity profile mainly being approximated by a quadratic function of depth. Bouhadef claims good agreement between measured and calculated jump radii, for a range of flow rates, but gives no details of these calculations. His measurement, by laser anemometry, of the velocity profile downstream of the jump is likewise only briefly described. His results suggest the existence, immediately behind the jump, of a 'wall-jet' profile. This finding is inconsistent with the presence of a reversed-flow region; and it seems likely that Bouhadef's measurements correspond to larger local Reynolds numbers, for which the separation eddy disappears (see § 4 following).

The present work reports on some new investigations of the circular hydraulic jump, which shed further light on its detailed structure and stability. Two series of experiments were performed using different apparatus, the first with rudimentary equipment and the second with more sophisticated instrumentation. These are designated experiments *A* and *B* respectively.

2. Experiment *A*

(*a*) *The apparatus*

A small constant-head tank was fitted with an outflow tube and nozzle which delivered a vertical laminar water jet. The flow rate could be adjusted by a screw clip fitted to the flexible tube. The jet was directed onto a horizontal glass plate set on the bottom of a rectangular Perspex fish tank. To facilitate complete wetting of the plate its edges were surrounded by absorbent paper laid flat on the tank bottom. The base of the tank and the plate had dimensions $29{\cdot}8 \times 19{\cdot}4$ cm and $8{\cdot}1 \times 10{\cdot}7$ cm respectively and the thickness of the plate was 0·15 cm.

The flow was started at a time $t = 0$ and complete wetting was quickly established (with manual assistance when necessary). As the liquid depth increased with time t, the radius r_1 of the circular hydraulic jump progressively decreased and its appearance assumed various forms. The times of onset of various characteristic features were recorded by stopwatch. Runs were made at various constant flow rates, which were measured both before and after each run by means of measuring jar and stopwatch. The jet emanated from the nozzle at a height of 16·2 cm above the plate. Two nozzle

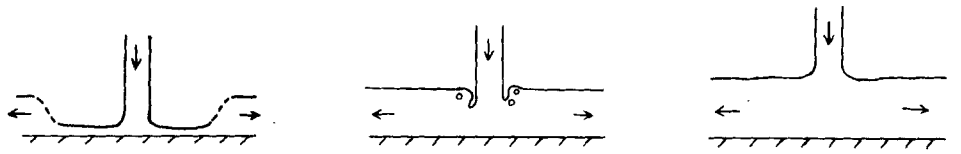

(*a*) $t_1 < t < t_2$ (*b*) $t_2 < t < t_3$ (*c*) $t > t_3$

FIGURE 1. Flow configurations. (*a*) Typical jump; (*b*) jump closed in on jet; (*c*) meniscus rises up jet. The vertical scale is exaggerated.

sizes were used, with internal diameters 6·15 mm and 2·11 mm. For a known flow rate, the mean liquid depth above the plate at each instant t is readily calculated, on making appropriate allowance for the small height of the plate above the tank bottom. Since the area within the circular hydraulic jump was small compared with that of the tank bottom, this mean depth is virtually the depth outside the jump.

The diameter of the jet at impact could not be measured with the tank in position. Accordingly, separate measurements at the appropriate location were made with the tank removed, for various flow rates, using a travelling microscope. In all cases for which measurements were made, no substantial variations due to capillary instability were present. The jet diameters with and without the tank were effectively identical for the jets used here, any upstream influence being confined to a few millimetres above the plate. Of course, at sufficiently low jet Reynolds numbers, a jet (of treacle, say) may meander, or coil, for some distance above the plate: but no hydraulic jump forms in such circumstances.

(*b*) *Observed features*

At early times t, the jump radius r_1 was relatively large and the liquid depth increased smoothly across the jump much as in Isigai *et al.*'s category (ii) (their category (i) was never observed by us), but with small capillary ripples standing just upstream of the main jump. The flow was laminar, stable and axisymmetric. As the outer depth increased with time, the radius r_1 decreased and, at a certain instant t_1, the jump became unstable. The instability took the form of temporally periodic fluctuations with a sometimes well-defined azimuthal wavelength around the circumference of the jump. The flow was then no longer stable nor strictly axisymmetric. The fluctuations within the jump region generated waves which propagated radially outwards.

As the outer depth further increased, the radius continued to decrease and the oscillations became more violent with fewer 'wavelengths' visible around the circumference. At sufficiently large flow rates, but not at lower ones, air bubbles were entrained by the oscillations (cf. Isigai *et al.*'s case (iv)). Eventually, the oscillations reached the jet and, a short time later at time t_2, the whole jump closed in around it. The oscillations and the radiating waves then virtually disappeared but bubble entrainment might persist. Finally, at time t_3 the meniscus 'jumped up the jet' (see sketch in figure 1) and bubble entrainment ceased. Sporadic bubble entrainment thereafter was attributed to stray disturbances within the jet. Rather irregular deformations of the free surface near the jet remained visible, but the jump had gone.

Videotape recordings were made and these were used to confirm the objectivity of decisions regarding the various transition times. Oblique lighting was used to give enhanced contrast, the surface deformations casting light and dark 'shadows' on

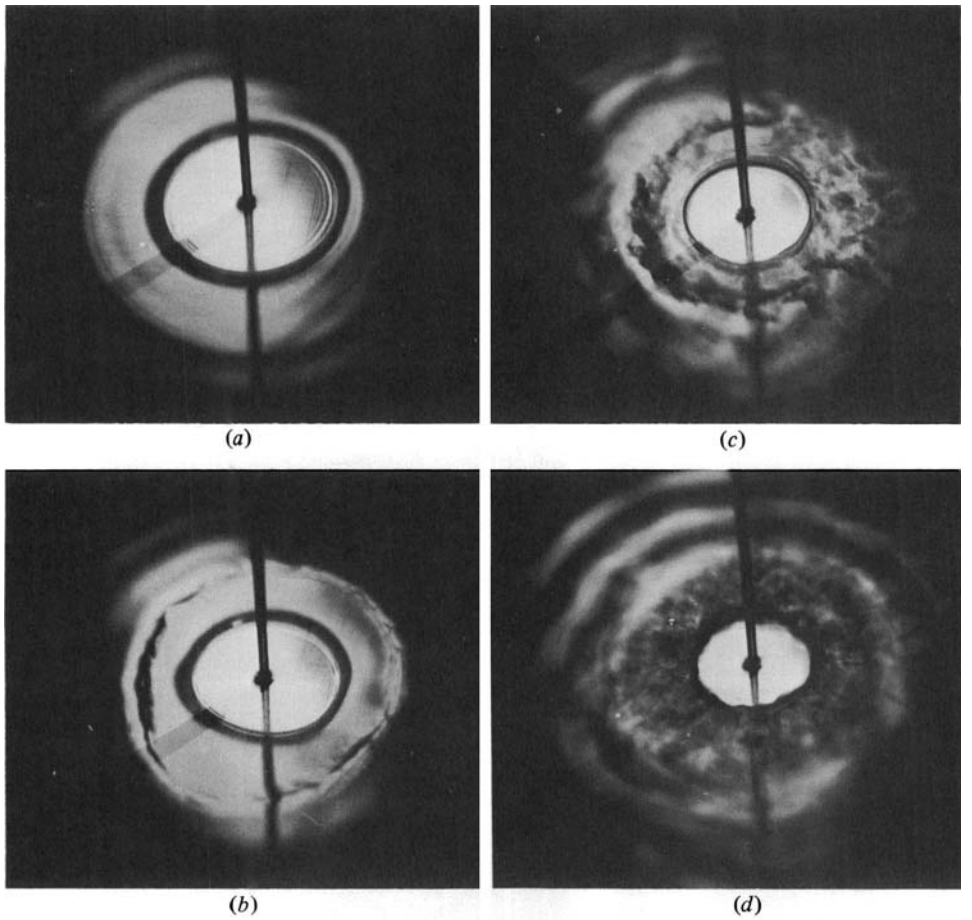

FIGURE 2. Time sequence of photographs from experiment B as outer depth increases. (*a*) stable jump; (*b*) stable jump with weakly fluctuating 'outer ring'; (*c*) oscillatory instability of jump begins; (*d*) strong oscillations with radiating waves. Larger grid squares are 1 cm². Surface features are directly visible by reflection of light.

squared paper stuck to the underside of the tank bottom. The same sequence of phenomena was observed using the different apparatus of experiment B. Photographs of this sequence are shown in figures 2 and 3. Those of figure 2 were taken during experiment B, the surface features there being more directly visible by reflection of light; those of figure 3 are enlargements of 'shadow' photographs from experiment A, which show the later stages and eventual disappearance of the jump. Note the total absence of radiating waves before onset of instability and the reduction of wave activity in figure 3 (*d*) when the jump has disappeared.

(*c*) *Measurements*

Given the volumetric flow rate Q and the onset times t_1, t_2, t_3, the mean water depth d associated with each transition is readily found from the formula $d = Qt_i/A$, where A is the area of the tank bottom. (To allow for the fact that the plate was 0·15 cm thick, either a little water was added prior to each run or a correction was made to the above formula. Errors so incurred were probably no larger than those associated with

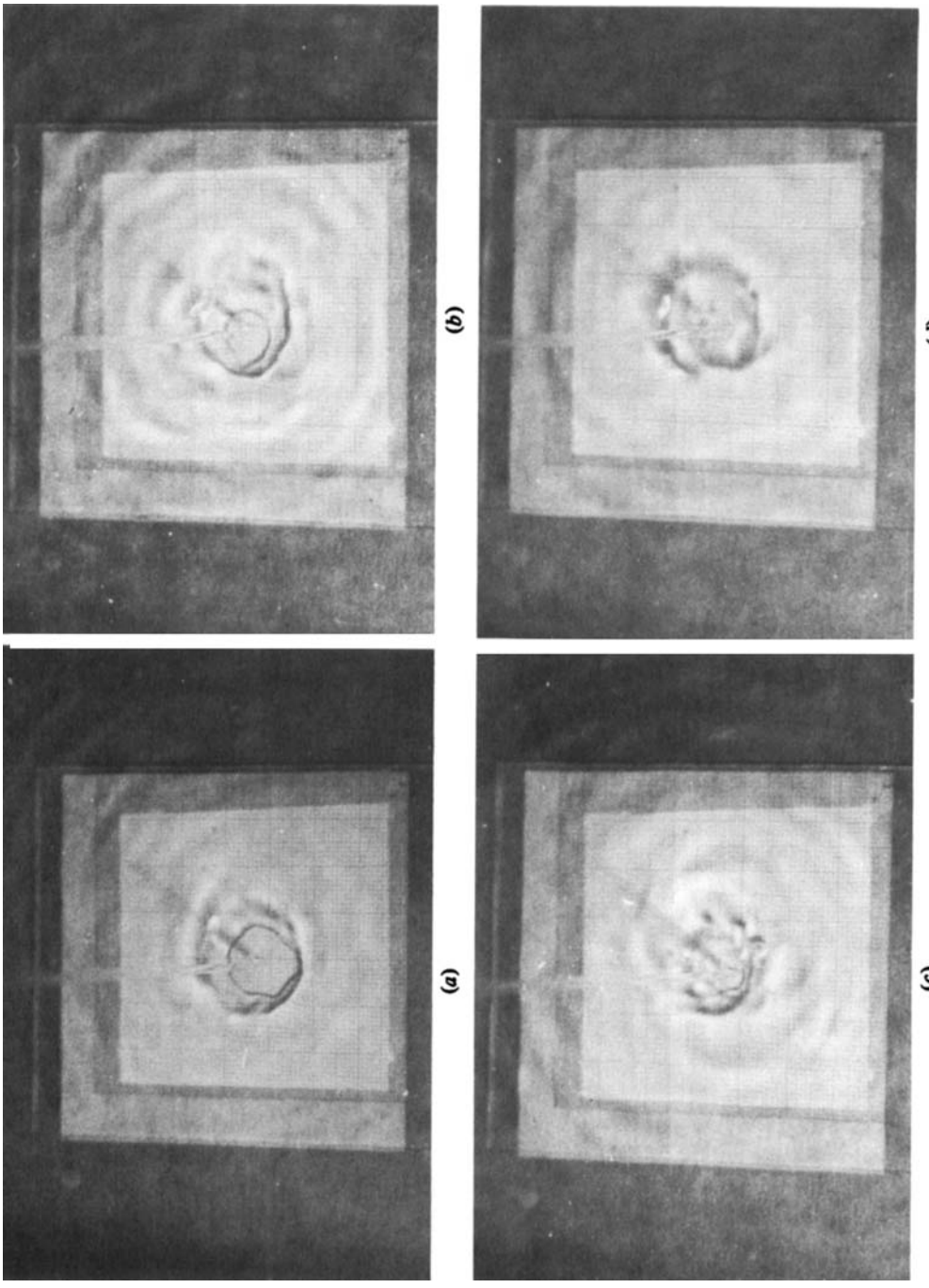

FIGURE 3. Time sequence of photographs from experiment *A* of later stages of jump as outer depth increases. (*a*) and (*b*) strong oscillations and radiating waves; (*c*) jump almost reaches jet (note bubble entrainment); (*d*) meniscus rises, jump and waves disappear. The larger grid squares are 1 cm^2. Surface features show as shadows on bottom of the glass plate.

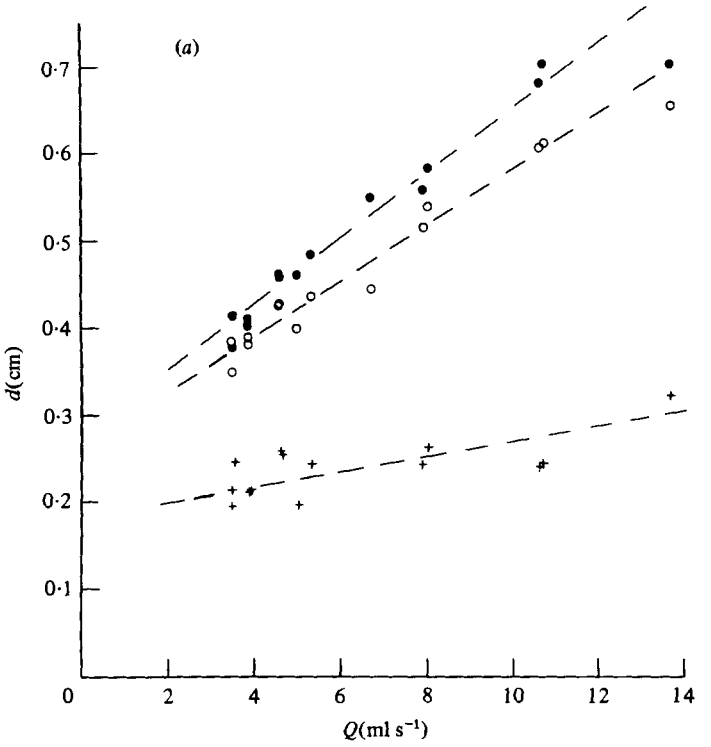

Figure 4(*a*). For caption see p. 354.

measuring onset times and flow rates.) Results were plotted of flow rate Q versus calculated depth d for the three transitions identified at times t_1, t_2 and t_3. These are shown in figures 4(*a*, *b*) for nozzle diameters 6·15 mm, 2·11 mm respectively.

The measured jet diameter at a distance of 16·2 cm below the nozzle is shown in figure 5 versus flow rate Q for both nozzles. The substantial scatter is mainly due to difficulty in making accurate measurements with the travelling microscope: but calipers proved no more satisfactory. It may be deduced that, at the same flow rate, the ratio of jet impact velocity with the small nozzle to that with the larger varies from about 1·5 at $Q = 4$ cm^3 s^{-1} to around 2·1 at $Q = 11$ cm^3 s^{-1}. A simple theoretical model of the variation of jet radius a with flow rate Q and nozzle height H proved inadequate and so is not described.

Results for the onset of instability at time t_1 in figures 4(*a*, *b*) show quite close agreement despite the differing nozzle sizes. Since the Froude numbers of the incoming flows are different for the two nozzles at the same flow rate, Isigai *et al.*'s proposal of the Froude number as a governing parameter appears to be inappropriate.

The 'closing up' of the jump on the jet at time t_2 and its final disappearance at time t_3 occur at larger depths and times with the smaller nozzle than with the larger (for equal flow rates Q). In other words, the jump moves inwards more slowly against the higher flow velocity.

This experiment was conducted with rather low flow rates Q in the range 3 to 14 cm^3 s^{-1}. The jet Reynolds number R in such cases varies between 5000 and 10000.

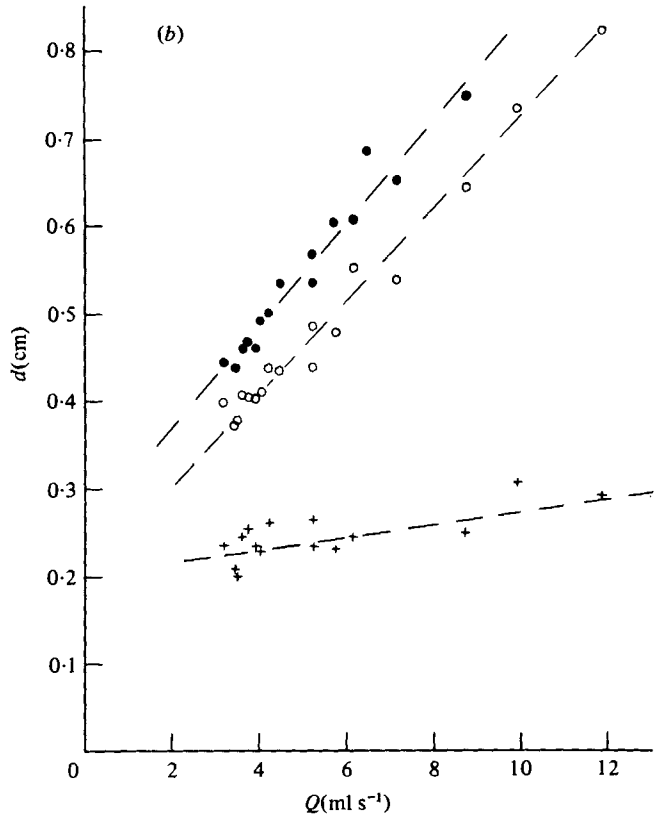

FIGURE 4. Flow rate Q versus outer depth d at transitions t_1, t_2, t_3. +, onset of instability: ○, jump closes on jet; ●, meniscus rises. Nozzle diameter is (*a*) 6·15 mm and (*b*) 2·11 mm.

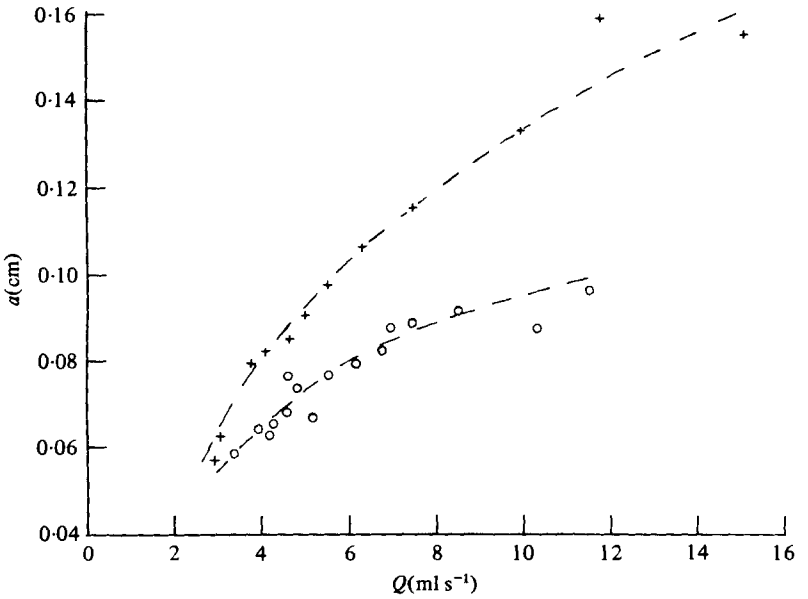

FIGURE 5. Measured jet radius a at plate position 16·2 cm below nozzle. Nozzle diameter: +, 6·15 mm; ○, 2·11 mm.

3. Experiment *B*

(*a*) *The apparatus*

This second experiment was designed to allow direct measurement of the liquid thickness across the jump region, for a steady flow. The availability of a larger flow rate also permitted investigation of higher Reynolds numbers than in experiment *A*. A light absorption technique was chosen to measure liquid thicknesses, the operating liquid being water to which a known quantity of methylene blue dye had been added. A helium–neon laser was shone from beneath a glass plate in the bottom of the apparatus, passing vertically through the glass and the dyed water upon it, and then into a detector. The detector was connected to a chart recorder which registered the intensity of the emergent beam. Laser and detector were mounted on the same vertical stand which could be moved horizontally in an arc of a circle at constant rate by a slow-speed electric motor. This enabled the laser–detector combination to track across the liquid from quite close to the incident jet to positions beyond the jump, giving a continuous record of beam intensity.

If I_0 denotes the beam intensity on passing through the glass plate alone, and I denotes that on passing through the plate and a liquid film of thickness h, it is to be expected that

$$I = I_0 e^{-\alpha h} \tag{3.1}$$

where α is an absorption coefficient which depends only on the dye concentration. Values of α appropriate to given concentrations were determined by calibration, using known volumes of dyed water in a glass dish. It follows that $h = \alpha^{-1} \ln (I_0/I)$, and so the thickness is known. Since the thickness typically varies from around 0·1 mm to about 2·5 mm across the jump region, the absorption coefficient had to be chosen with some care. Too low a coefficient gives little reduction in intensity for the thinner films and too high a coefficient allows little light to penetrate the thicker ones.

The remainder of the apparatus was as follows. A large head tank with adjustable outlet tap was connected to a flexible pipe and 12 mm diameter nozzle. From this nozzle emerged the jet which fell vertically onto the horizontal glass plate mentioned above. This plate was sealed into an aperture cut from the base of a shallow square metal tank. This plate and tank assembly was mounted on stands to enable easy adjustment of height. From each corner of the tank small pipes led to a central manifold from which the water emerged into a small collecting reservoir. A pump returned the water to the head tank when required. The volumetric flow rate of the jet was determined using stopwatch and measuring jar both before and after each run. The diameter of the jet just before impact with the plate was estimated (to within about 10 %) using calipers. To prevent formation of dry patches at the edges of the plate and to facilitate an even flow of liquid from the plate, absorbent paper was usually placed flush with the edges. Reasonably constant operating conditions could be maintained for as long as was required and external vibrations were eliminated as far as possible.

(*b*) *Liquid thickness measurements*

From chart recordings of light intensity, scanning across the flow, profiles of the liquid thickness across the jump could be deduced from the absorption law (3.1). The water surface in the head tank was kept at approximately 46 cm above the nozzle outlet. The vertical distance from nozzle to plate could be varied. Results were

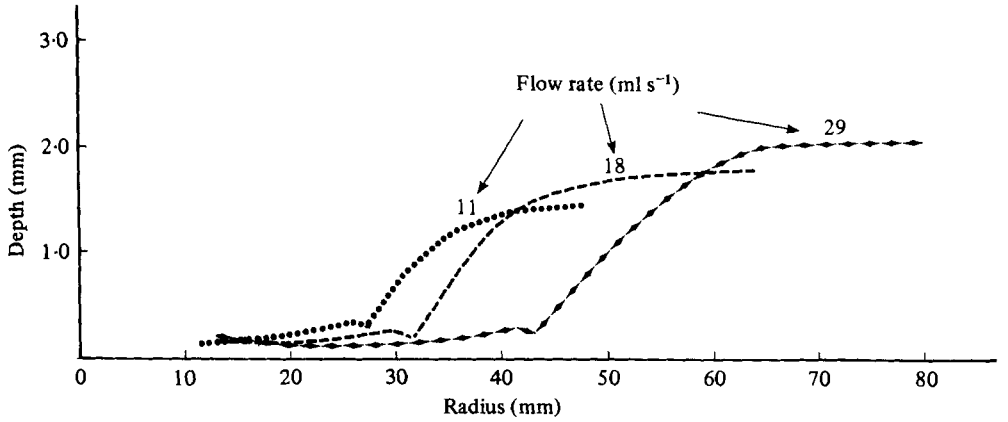

FIGURE 6. Typical liquid depth profile across jump in stable regime. Nozzle height is 19 cm. Flow rates are as indicated.

obtained for different distances and various constant flow rates. Unfortunately, there was no satisfactory means of controlling, independently, the liquid depth downstream of the jump.

Typical results are shown in figure 6 for three different flow rates. For these cases shown, the jump was stable and axisymmetric. The small rise and dip just before the jump was due to a standing capillary ripple. (This is also visible in photographs (*a*) and (*b*) of figure 2.)

Further measurements were made of jump radius and of depth just upstream and downstream of the jump, at various flow rates. In some of these cases, the jump was unstable and, because of the oscillations, the jump profile could not be determined. However, the mean depth just downstream of the jump remained clearly defined. Some of these results were obtained under unsteady conditions, with the tank allowed to fill gradually with water, much as in experiment *A*. This was done to achieve a range of jump positions and outer depths for fixed flow rates. Some measured data are shown in table 1, along with the quantity $2\pi v = Q/r_1 d$ where v estimates the mean liquid velocity just behind the jump. Direct measurements of v were not made. In fact, the slow flow some distance downstream of the jump was never truly axisymmetric: meanders and almost stagnant regions occurred doubtless because the water did not flow sufficiently uniformly from the edges of the plate. But this irregularity had little effect on the flow near the jump. The position of r_1 was that where the depth was estimated to be $\frac{1}{2}d$. The inner depth h just ahead of the jump was in the range 0·1 to 0·2 mm, but accuracy here was poor since a low dye concentration was used to yield accurate values of d.

The data of table 1 were compared with Watson's theoretical results (1.2*a*, *b*) by plotting the logarithm of the left-hand side of these equations against $\log[(r_1/a)\,R^{-\frac{1}{3}}]$. As Watson also found, many points lie far below his theoretical curve, the most distant ones usually having the smallest values of r_1/d. Our measured values of r_1 range from 0·8 cm to 4·0 cm as compared with Watson's higher range of about 2·5 cm to 17 cm. For this lower range, it was clear that Watson's theory gives a poor estimate of r_1.

It is seen from table 1 that the calculated velocity v varies rather slowly with Q and d. Corresponding data with the nozzle height reduced to 12 cm yielded rather

Flow rate Q (ml s^{-1})	Jet radius a (mm)	Jump radius r_1 (cm)	Outer depth d (mm)	Velocity $2\pi v = Q/r_1 d$ (cm s^{-1})
4·48	1·0	1·2	1·8	20·7
		1·0	2·3	19·5
		0·8	3·5	16·0
7·87	1·3	1·7	1·9	24·4
		1·5	2·2	23·8
		0·8	3·5	28·1
11·6	1·55	2·3	2·2	22·9
		2·1	2·4	23·0
		1·4	3·0	27·6
19·8	1·8	3·2	2·2	28·1
		3·05	2·4	27·0
		2·3	3·5	24·6
26·0	2·15	4·0	2·1	31·7
		3·6	2·5	28·9
		2·3	3·3	34·0

TABLE 1. Measurements for nozzle height 17 cm.

similar results, but with somewhat smaller r_1 (and hence greater v) than for the height of 17 cm at the same values of Q and d. Attempts to find a satisfactory empirical correlation of the flow quantities were unsuccessful. Three independent dimensionless parameters (R, d/a and ga^5/Q^2, say) are involved, even when surface tension is ignored, and one parameter r_1/d which depends on all three; given our limited data this lack of success is hardly surprising. With a fixed nozzle size and height, a and Q are no longer independent quantities. In such cases, an empirical curve of v versus Q, chosen to fit measured data, might give a reasonably satisfactory means of predicting r_1, given Q and d.

(*c*) *Instability measurements*

To complement the measurements of experiment A relating to the onset of oscillatory instability, data were obtained on flow rate, jump radius and liquid depth just inside and outside the jump at onset. As before, the tank was allowed to fill slowly at a constant rate until the instability appeared. A typical time-sequence of photographs is shown in figure 2. It was noticed that, before onset of the vigorous oscillations at the jump, an 'outer ring' associated with a further very small change in depth appeared some distance downstream. This is clearly visible in figure 2(*b*). This outer ring was usually somewhat irregular, as in figure 2(*b*), when it fluctuated in a weak, fairly random, manner very different from the later periodic oscillations of the jump. Occasionally, even when stable, it was elliptic rather than circular in shape; this was so when the flow downstream of the jump was particularly asymmetrical. Such a flow could be produced deliberately by blocking two of the four outlet pipes; but it also occurred spontaneously, due to uneven flow from the glass plate. The explanation of this outer ring is given in (*d*) below. As the outer depth increased, this outer ring decreased faster than the jump radius r_1 and the oscillatory instability set in at about the time that the two came together. As well as examining the onset of the oscillatory instability of the jump, an attempt was made to record the onset of the much weaker fluctuations associated with the outer ring. This latter occurs before

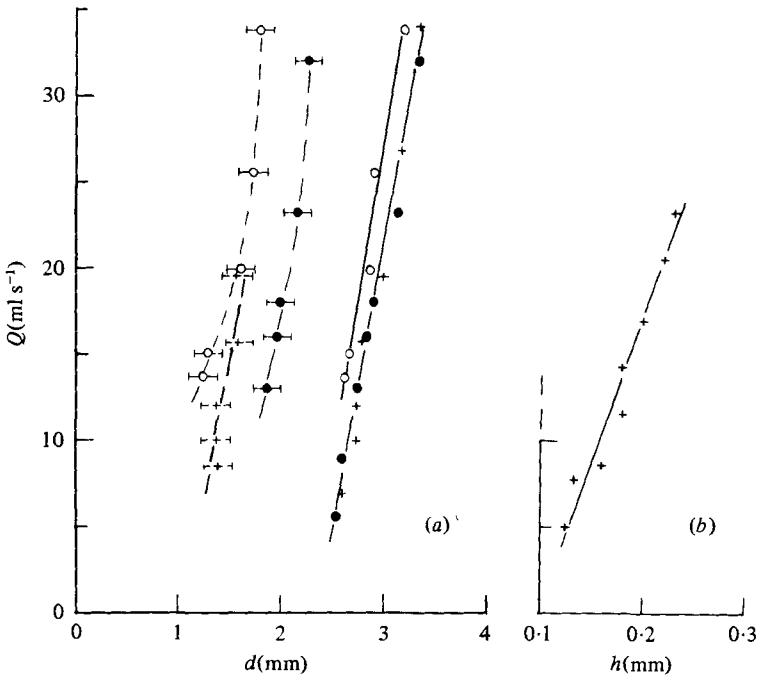

FIGURE 7. (*a*) Outer depth d and (*b*) inner depth h versus flow rate Q at onset of instabilities. Points enclosed by ⊢ ⊣ denote onset of irregular fluctuations of the 'outer ring'; remaining points refer to onset of oscillatory instability of the jump. Nozzle height: ●, 12 cm; +, 19 cm; ○, 28·5 cm.

the oscillatory instability, as the tank slowly fills; but its detection was inevitably rather subjective and imprecise.

Observations of the onset of these two transitions are recorded in figure 7 (*a*), which shows flow rate Q against outer depth d for three different nozzle heights; and in figure 7 (*b*), which shows Q against the depth h just inside the jump at onset of the oscillatory instability for a single nozzle height. The errors in measuring h may here be as great as 20 %, but those in d are much less. The outer depths at onset for the two lower nozzle heights are indistinguishable; those for the greatest height are slightly smaller.

Measurement of jet diameter $2a$ at the plate position was made using calipers. Though accuracy was poor, the following results may be taken as typical. At a flow rate Q of 30 ml s^{-1}, $2a$ was approximately 5 mm, 4·3 mm, and 3·9 mm at respective distances of 12 cm, 19 cm and 28·5 cm below the nozzle; while, with Q = 10 ml s^{-1}, $2a$ was about 2·8, 2·6 and 2·3 mm at these same distances.

Figure 8 shows flow rate Q versus radius of jump r_1 at onset of oscillations for various nozzle heights from 12 cm to 28·5 cm. Remarkably, no consistent variation with nozzle height could be detected and the scatter of results accords with the expected errors in measuring r_1 at onset. These results lie closely about the line $r_1 = 0{\cdot}34 + 0{\cdot}108Q$ in the chosen units, over a wide range of Q. The small scatter is evidence of the sharpness of the transition from 'almost steady' to oscillatory flow.

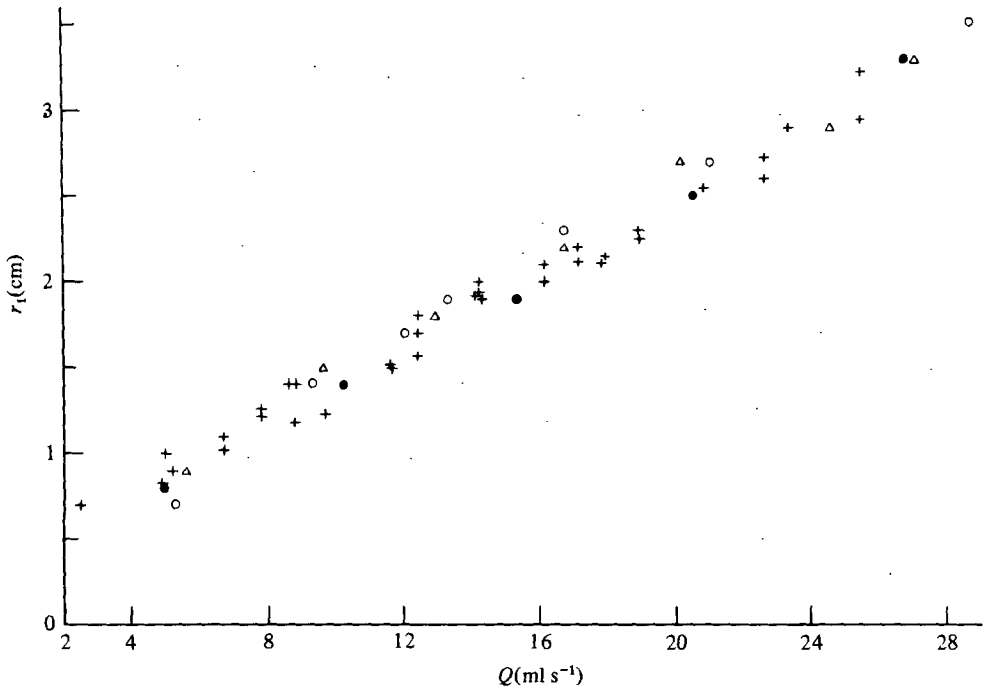

FIGURE 8. Jump radius r_1 versus flow rate Q at onset of oscillatory instability, for various nozzle heights H. ●, H = 12 cm; △, H = 19 cm; ○, H = 28·5 cm; +, various values within this range. Additional data points not shown are r_1 = 3·7, Q = 33·3 (H = 19) and r_1 = 4·5, Q = 43 (H = 12).

(*d*) *Flow visualization*

To investigate further the flow structure near the jump, careful visual observations were made using undyed water containing a quantity of 'Mearlmaid' pearl essence. This preparation, used in the cosmetics industry, consists of minute 'platelets' rather like tiny fish scales: it is here preferable to aluminium flakes for flow visualization because of its lower density. Appropriate lighting and close scrutiny enabled the motion of individual 'platelets' of the additive to be followed.

Prior to the onset of oscillatory instability, a substantial region of reversed flow was seen. This stretched from the jump in depth downstream to the 'outer ring'. That the reversed flow occurred next to the wall was confirmed by smearing small quantities of poster paint onto the plate: this moved upstream or downstream according to whether it was placed before or beyond the 'outer ring'. The 'outer ring' is visible in figure 2(*b*) because a tiny change in surface slope is brought about by reattachment of the flow behind a long 'eddy' which extends downstream from the jump. The existence of the reversed flow region was also detected by Nakoryakov *et al.* (1978), as mentioned in the introduction.

The rapid flow ahead of the jump *remains rapid for some distance behind it* by separating from the wall and riding over the slower-moving fluid in the eddy. That the boundary layer should separate is due to the sudden adverse pressure gradient associated with the hydrostatic pressure beneath the rapidly changing depth at the jump. This was first pointed out by Tani (1949); however, one cannot go all the way

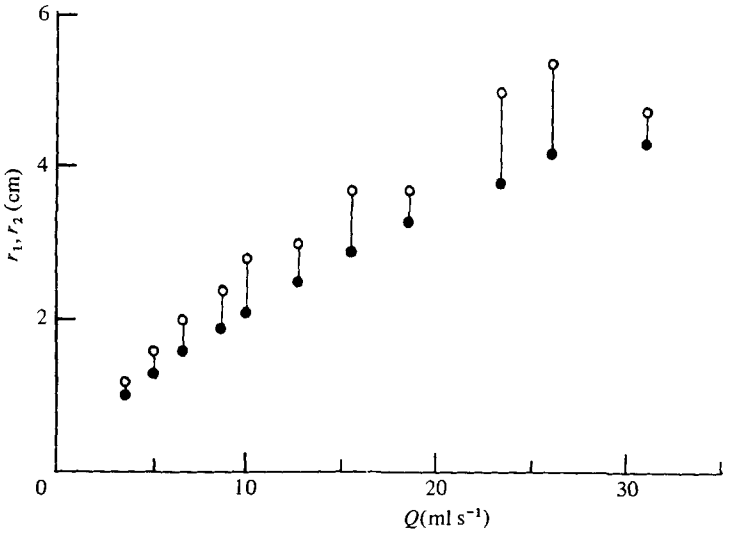

FIGURE 9. Typical variations of jump radius r_1 and radius of reattachment line r_2 versus flow rate Q with uncontrolled outer depth. The solid lines denote lengths of closed eddy. Measurements of r_2 are rather rough owing to some asymmetry. At $Q = 31$, r_2 showed fluctuations. On further increasing Q, r_2 merged with r_1 and oscillatory instability ensued.

with him in identifying the jump as essentially a boundary-layer separation phenomenon.

The flow is gradually retarded by continuing viscous action: in particular, individual particles do *not* experience a sudden reduction in velocity on passing through the jump. To this extent, the term 'circular hydraulic jump' is a misnomer. The flow within and around the eddy is an essential part of the phenomenon; and the eddy may extend to radial distances almost twice that of the jump radius, though it is usually rather shorter.

As the outer depth is allowed to increase, at fixed flow rates, the eddy shortens; and, when it shrinks right up to the jump itself, the oscillatory instability begins. It proved impossible to make satisfactory simultaneous measurements of changing eddy length and jump radius in this situation: the 'outer ring' was frequently rather asymmetric and itself displayed a weak instability (as mentioned above). However, some typical values of jump radius r_1 and approximate reattachment radius r_2 were recorded under steady conditions at different flow rates Q, where the water was left to flow naturally from the plate with the outer depth uncontrolled. These are shown in figure 9; but no great accuracy is claimed for the estimates of r_2. At $Q = 31$ ml s^{-1} the 'outer ring', or reattachment line, showed the weak instability. When the flow rate was increased further, the oscillatory instability began.

4. Discussion

The flow structure described above is shown schematically in figure 10. It is only when the eddy shrinks in size that anything approaching a genuine discontinuity of velocity exists. However, even with a long eddy, considerations of mass conservation and momentum balance across the rather sudden depth change must still apply. But the vertical structure of the flow now plays a crucial role: mass and momentum

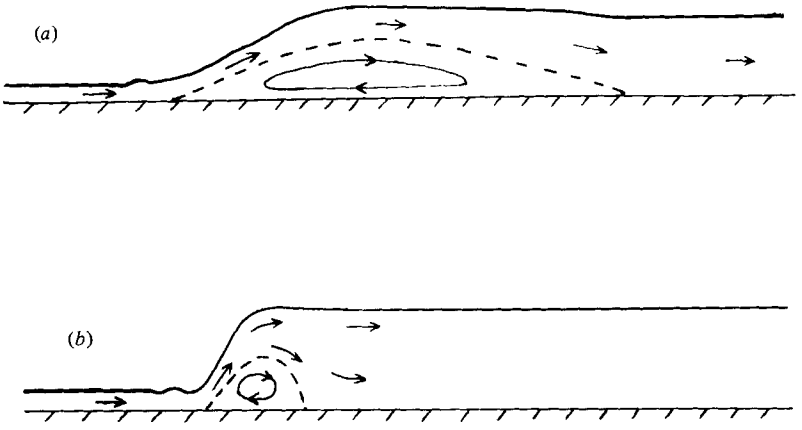

FIGURE 10. Flow structure (*a*) with long eddy, (*b*) with short eddy just before onset of oscillations; inferred from visualization studies. The vertical scale is exaggerated.

requirements are met, in the first instance, by the changed velocity profile associated with separation. Unlike the case of the classical hydraulic jump, there is here no need to suddenly 'get rid' of excess energy by enhanced local dissipation or backwards radiation of wave energy through standing cnoidal waves. Instead, the flow gradually loses its energy over the substantial length of the eddy region; reattachment is the inevitable consequence of the absence of a pressure gradient.

Just why the eddy shortens as the outer depth increases is still unknown, and poses a novel problem in boundary-layer theory. But, once it has shrunk to zero, the usual jump conditions associated with a discontinuous hydraulic jump (see, for example, Lighthill 1978) must more or less apply, in the modified form of Watson (1964). Now, energy must be lost at a finite rate from the immediate vicinity of the jump. Enhanced viscous dissipation by bubble entrainment and frothing is a possibility and must certainly occur in sufficiently strong jumps. But the jumps observed here employ a more orderly means. The oscillatory instability not only causes increased local dissipation by generating azimuthally varying motion: more importantly, it generates capillary–gravity waves which radiate outwards, carrying away energy. Whereas, in the classical hydraulic jump, it is *standing* cnoidal waves which shed energy downstream, this option is not open in the present context. This is because the group velocity of capillary–gravity waves *exceeds* the phase velocity and so any waves standing against the radial flow must transmit energy *upstream* instead of downstream. If such waves are to transmit energy downstream, then their phase velocity must also be directed downstream and they must be generated by a temporally oscillating source. The observed azimuthal wavenumber around the jump almost certainly depends on surface tension. It is an easy calculation to show that capillary–gravity waves with realistically small amplitudes are capable of transporting all the excess energy away from the jump. The oscillatory instability of the jump comes to seem inevitable.

The onset of instability may be identified with a critical Reynolds number R_c. The local Reynolds number appropriate to a given radius r is $Q(2\pi r\nu)^{-1}$. We now define a Reynolds number R_j, typical of conditions just ahead of the jump at $r = r_1$, by choosing r to be r_1 *minus* 0·34 cm. The line $r_1 = 0{\cdot}34 + 0{\cdot}108Q$, which was found

to fit the instability data of figure 6, then corresponds to a critical value of $R_c = 147$ for R_j on taking ν to be 0·01 cm^2 s^{-1}. The jumps investigated were stable or unstable according as R_j was less or greater than 147, the length of the closed eddy decreasing as R_j increased: this behaviour is the opposite of that of steady eddies behind bluff bodies, which increase in length as the Reynolds number increases. Further experiments with different liquid viscosities are desirable to reinforce this Reynolds number criterion. The alternative possibility of a critical local Froude number $Fr = V(gh)^{-\frac{1}{2}}$, where $V = Q(2\pi r_1 h)^{-1}$ and h is the inner depth, is inconsistent with the experimental data of figures 7 (*b*) and 8.

Experiment *A* was carried out by R.L. as an undergraduate vacation project supported by the Yapp Trust and supervised by A.C. Experiment *B* was mostly carried out by M.F. as a project in Honours Physics, jointly supervised by A.C. and P.G. The technical resources of the University of St Andrews Physics Department are gratefully acknowledged.

REFERENCES

BOUHADEF, M. 1978 *Z. angew. Math. Phys.* **29**, 157–167.

CHAUDHURY, Z. H. 1964 *J. Fluid Mech.* **20**, 501–511.

ISHIGAI, S., NAKANISHI, S., MIZUNO, M. & IMAMURA, T. 1977 *Bull. J. S.M.E.* **20**, 85–92.

LIGHTHILL, M. J. 1978 *Waves in Fluids*. Cambridge University Press.

NAKORYAKOV, V. E., POKUSAEV, B. G. & TROYAN, E. N. 1978 *Int. J. Heat Mass Transfer* **21**, 1175–1184.

OLSSON, R. G. & TURKDOGAN, E. T. 1966 *Nature* **211**, 813–816.

TANI, I. 1949 *J. Phys. Soc. Japan* **4**, 212–215.

WATSON, E. J. 1964 *J. Fluid Mech.* **20**, 481–499.